

ON-DESIGN SOLUTIONS OF HYPERSONIC FLOWS PAST ELLIPTIC-CONE DERIVED WAVERIDERS

Bok-hyun Yoon*

(Received September 5, 1991)

The hypersonic flows past a class of elliptic-cone derived waverider at the on-design condition are analyzed. A CFD (Computational Fluid Dynamics) algorithm due to Lawrence is utilized to numerically integrate the steady Euler equations. The singular behavior at the sharp leading-edge of a waverider where a bow shock is to be attached for the ideal situation makes the computation extremely difficult for convergence of numerical solutions. Various types of grids are generated and tested for converged solutions. A new formula for more accurate waverider shape is established and by means of this new waverider configuration the reason for the shock stand-off which was detected in previous investigations is clarified in this paper.

Key Words: Waverider, Hypersonic Flow, CFD, Shock Wave, Grid Generation, Singular Behavior

NOMENCLATURE

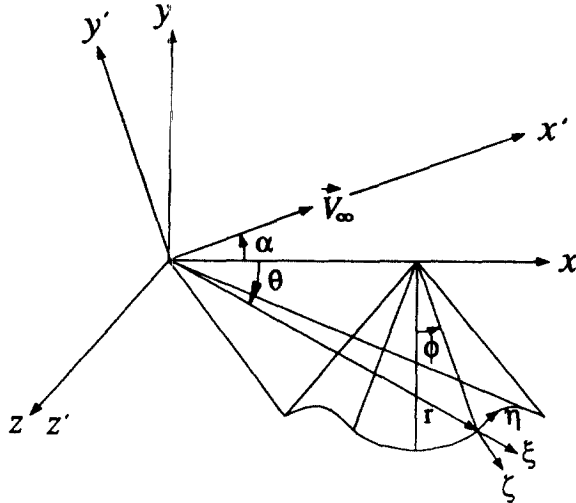
e	: Parameter defined as $e \equiv -\varepsilon \frac{w(\delta)}{\delta V_\infty}$
$\bar{e}_\theta, \bar{e}_\phi$: Base vectors in θ and ϕ -directions
F	: Surface function for lower portion of waverider
g	: Shock eccentricity parameter for elliptic cone
K_δ	: Hypersonic similarity parameter ($\equiv M_\infty \delta$)
M_∞	: Freestream Mach number
\bar{n}	: Outward unit normal vector
ξ	: Streamline displacement vector
v, w	: Perturbed velocity components (θ, ϕ) of basic cone in spherical coordinates
\vec{V}_∞	: Freestream velocity
\vec{V}	: Velocity vector
β	: Shock angle
δ	: Half cone angle
Δ	: Waverider leading edge angle
ε	: Small perturbation parameter
σ	: Ratio of β to δ
θ	: Conical angle
$\theta_o(\phi)$: Stretched variable
θ_c	: Conical angle of circular cone
θ_s	: Conical angle of bow shock
ϕ	: Azimuthal angle
ϕ_s	: Anhedral angle of waverider

1. INTRODUCTION

The design of trans-atmospheric and aero-space vehicles has been of great interest in recent years. The National Aero-Space Plane (NASP) of the United States of America is an example of the current effort to develop technologies to design a vehicle that will fly into orbit while taking off and landing like a conventional airplane. One concept for the

design of the forebody part of such a configuration is that of a waverider. A waverider shape offers a high lift and a small drag, and in addition, provides favorable flow properties for the inlet of the scramjet propulsion unit. A waverider is constructed by identifying the stream surfaces of known supersonic flow fields as new solid surfaces that are connected in such a way as to form a new aerodynamic configuration. The flow field and aerodynamic properties of the waverider configuration are thus well known from the basic flows from which they were obtained. This basic flow and geometric configuration are called the on-design conditions (Mach number $M_\infty=4$, angle of attack $\alpha=0^\circ$). When the waverider shape is held fixed, and either or both of the Mach number and orientation of the oncoming flow are varied, the varied conditions are said to be the off-design conditions. The development of Computational Fluid Dynamics (CFD) possibly provides the only practical means for studying the off-design properties of waverider configurations. The first CFD analyses of waverider flow fields were made by Jones (Jones, 1986). These considered the elliptic-cone derived waveriders of Rasmussen (Rasmussen, 1980) for which experimental results were available. The CFD calculations associated with Jones were simplified by using the full potential equations to describe the flow fields. However, the irrotational assumption involved in the potential equations is not appropriate for general hypersonic flows, since rotationality is one of the important features of hypersonic flows. Just recently, after the completion of the present work, several other papers (Long, 1990, Jones, Dougherty, 1990, Lia, Isaac, Miles, 1990) have appeared that deal with the calculation of waverider flow fields by CFD methods. These studies used existing codes based on unsteady 3-D equations with super computers like the Cray-2. But for those problems the use of unsteady equations is not effective and economical, since they deal with steady states. The computational dimension in those studies requires one more (time dimension) than the necessary number and this approach demands higher cost in respect of computer storage and computing time. On the other hand, attempting steady equations requires much more

*Department of Mechanical Engineering, College of Engineering, Mokpo National University, #61 Dorim-ri, Chyungge-myun, Muan-gun, Cheonnam 534-729, Republic of Korea



$(x, y, z) = \text{Cartesian}$

$(r, \theta, \phi) = \text{Spherical}$

$(\xi, \eta, \zeta) = \text{Body-fitted}$

Fig. 1 Waverider and coordinate systems

troublesome efforts with regard to numerical integrating techniques. In this investigation the steady euler equations are numerically integrated for waverider flow fields with no irrotational assumption. Fig. 1 shows a waverider sketch with three coordinate systems used for the problem. A comprehensive study for the hypersonic flows past a class of elliptic-cone derived waverider at both on-design and off-design conditions has been carried out by the author (Yoon, 1990). However, in this paper only its on-design solution is presented. Some of the main goals include examining the reason for the shock stand-off at the leading-edge, overcoming the difficulty of singularity due to the attached shock at the sharp tip, and constructing desired grids for a converged solution. In addition, a new waverider configuration for the required shock attachment at the on-design condition is established.

2. WAVERIDER

An elliptic-cone derived waverider is constructed by the flow field past an elliptic-cone which is formed by the perturbation expansion of a circular cone. To describe such a waverider we use polar coordinates (r, θ, ϕ) in Fig. 1.

2.1 New Formula of Waverider

Model-1 waverider is represented by the following equation (Jischke, Rasmussen, Daniel, 1983)

$$\frac{\theta(\phi)}{\delta} = \frac{\theta_c(\phi)}{\delta} + \left[\frac{\theta_s(\phi)}{\delta} - \frac{\theta_c(\phi)}{\delta} \right] \left[\frac{\tan \phi}{\tan \phi_s} \right]^{1/e} \quad (1)$$

where the subscripts s and c are for the bow shock around an elliptic cone and the basic circular cone, and δ is a half cone angle. This equation describes the conical stream surfaces

generated by hypersonic flows past elliptic-cones. It is valid for small eccentricities, that is, for small ϵ . e is a parameter determined by ϵ and the azimuthal velocity component w and some other variables, whose values for specific waveriders will be presented in a subsequent subsection. Since all of the streamlines that comprise a conical stream surfaces pass through a common ray along the conical shock, they all have the same entropy. Thus, a conical stream surface is also a constant-entropy surface. A better representation for a conical stream surface can be obtained by approximating the combination $w(\theta_0)/(\theta_0 + \delta)$ by a linear variation with θ_0 from the body to the shock, where θ_0 is a new stretched variable (Rasmussen, 1991) defined as

$$\frac{\theta_0 - \delta}{\beta - \delta} = \frac{\theta - \theta_c(\phi)}{\theta_s(\phi) - \theta_c(\phi)} \quad (2)$$

Thus we obtain (Yoon, 1990)

$$\left(\frac{\theta_0 - \delta}{\beta - \delta} \right) \exp \left[\left\{ \frac{2w(\beta)}{(\sigma+1)w(\delta)} - 1 \right\} \left(\frac{\theta_0 - \beta}{\beta - \delta} \right) \right] = \left[\frac{\tan \phi}{\tan \phi_s} \right]^{1/e} \quad (3)$$

where $\sigma \equiv \beta/\delta$. If the exponential term in this expression were ignored, then this result would lead to Eq. (1). Eq. (3) which is a new formula for waveriders is more accurate especially near the shock. In this paper the waverider related to Eq. (3) is said Model-2 waverider.

2.2 Construction of Elliptic-Cone Derived Waverider

A conical constant-entropy stream surface, such as given by Eq. (1) or Eq. (3), is used as a lower compression surface in a waverider configuration. The complementary upper freestream surfaces are taken to be a pair of triangular plane surfaces that pass through the axis of symmetry (x -axis) of the basic cone and intersect the elliptic-cone shock at the angle $\phi = \pm \phi_s$. A cross-section plane, perpendicular to the axis of symmetry, is shown in Fig. 2.

2.3 Waverider Models

Two basic elliptic-cone waveriders are considered, denoted by A and B . For both cases, the on-design Mach number is $M_\infty = 4$ and the eccentricity is $\epsilon = 0.1$. The following table

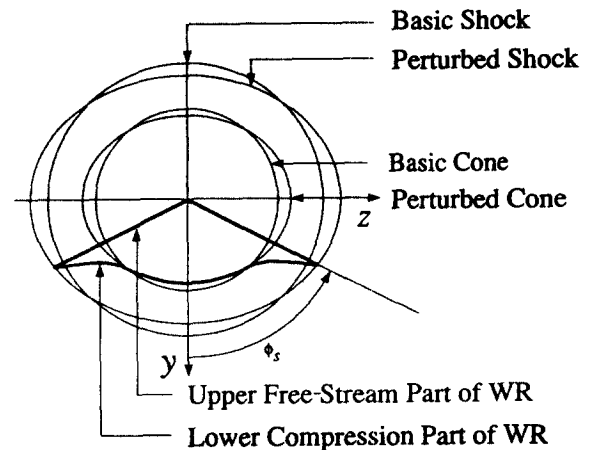


Fig. 2 Construction of elliptic-cone waverider

Table 1 Specifications of Model-A and B waveriders

Parameters	Waverider A	Waverider B
δ	12°	18.62°
ϕ_s	60°	70°
K_s	0.838	1.30
σ	1.62	1.34
g	0.382	0.597
$1/e$	6.132	7.611

shows the specifications for Model-A and B waveriders: where g is a shock eccentricity parameter for an elliptic-cone and $K_s (= M_\infty \delta)$ is the hypersonic similarity parameter. The parameters for Waverider B correspond to the shape tested in the reference (Jischke, Rasmussen, Daniel, 1983). Waverider A corresponds to the shape tested in the reference (Rasmussen, 1986), except that the eccentricity was $\varepsilon=0.05$ in the reference, which led to a corresponding value of $1/e=12.264$. This large value of $1/e$ produces a very sharp leading-edge on the waverider, and the initial efforts at calculating the flow led to numerical instabilities which were subsequently overcome. Consequently, the larger value of ε was selected for the present study.

2.4 Geometry of Waverider Leading-Edge

It is desired to determine the angle Δ between the upper planar surface and the lower compression surface. The outward pointing unit normal of compression surface is determined by $\hat{n} = \nabla F / |\nabla F|$, where $F(\theta, \phi) = \theta - \theta(\phi)$, where $\theta(\phi)$ is determined (Yoon, 1990) by the first order perturbations and hypersonic-small-disturbance theory (HSDT) for the stream line equation

$$\vec{V} \times d\vec{s} = 0 \quad (4)$$

For small polar angles, we have

$$\hat{n} = \frac{\hat{e}_\theta - \frac{1}{\theta} \frac{d\theta}{d\phi} \hat{e}_\phi}{\left[1 + \left(\frac{1}{\theta} \frac{d\theta}{d\phi}\right)^2\right]^{1/2}} \quad (5)$$

Since the outward normal to the freestream planar surface is \hat{e}_ϕ , we can determine the leading edge tip angle Δ (where $\theta = \beta$) by $\cos(\pi - \Delta) = \hat{n} \cdot \hat{e}_\phi$. It can then be determined that

$$\tan \Delta = \beta \left(\frac{d\phi}{d\theta} \right)_{\theta=\beta} = - \frac{\varepsilon w(\beta) \sin 2\phi_s}{V_\infty \delta \sigma \left(1 - \frac{1}{\sigma^2}\right)} \quad (6)$$

The third term is obtained by the vector equation for stream surfaces, Eq. (4). The azimuthal velocity at the shock can be

determined from the shock boundary conditions (Rasmussen, 1991):

$$\frac{w(\beta)}{\delta V_\infty} = - \frac{2g}{\sigma^2} \quad (7)$$

Thus the leading-edge tip angle is determined by

$$\tan \Delta = \frac{2\varepsilon g \sin 2\phi_s}{\sigma(\sigma^2 - 1)} \quad (8)$$

The tip angle according to the approximate formula Eq. (1) is determined by a different result. It is,

$$(\tan \Delta)_{approx} = \frac{e\sigma}{2(\sigma - 1)} \sin 2\phi_s \quad (9)$$

The tip angles for models A1 and B1 are determined by the approximate formula Eq. (9), whereas the tip angles for models A2 and B2 are determined by the correct formula Eq. (8). The numerical values are shown in the following table:

The models A1 and B1 with the compression surface described by the approximate formula Eq. (1) have considerably thicker angles than the corresponding correct waveriders would have.

3. PROBLEM CHARACTERISTICS & NUMERICAL INTEGRATION

The major difficulty involved in this problem lies in handling the singularity produced by the sharp leading-edge. A bow shock which exhibits another singular behavior is attached at the edge at the on-design condition in the ideal inviscid case. Considering the high lift-drag ratio of the waverider is from the confined flow of high pressure in the shock layer, the shock attachment is one of the main characteristics of waveriders. Therefore, it is important to examine the singular behavior at the tip and to identify the reason for the shock stand-off which was detected at earlier studies. For that purpose two types of waveriders, Model-1 and Model-2 according to different equations for the lower compression surface, are investigated. Another types of waveriders, Model-A and Model-B according to different hypersonic similarity parameters K_s are also studied. Thus for this problem, both grid generating and numerical integrating procedures should be carried out with great care in order to get successful results. A slightly deteriorated grid structure near the tip would result in the divergence of the numerical calculations. The whole computer code for the computational analysis of waverider flows is composed of three packages of program files. They are:

- (1) AGRID : generating grid
- (2) STARS3D : solving for flows
- (3) CPLOT : plotting various graphs and obtaining approximate solutions for waveriders.

AGRID, which was written by the author (Yoon, 1990), is the code producing body-fitted coordinates. This can generate algebraic, hyperbolic, and elliptic grids. The STARS3D code developed by Lawrence et al. (Lawrence, Tannehill, Chaussee, 1986) at NASA, is used to solve hypersonic flows past waveriders with various conditions. The STARS3D code is based on the Parabolized Navier-Stokes equations (PNS) which are numerically integrated by the space marching

Table 2 Waverider leading-edge angles

Model	Δ
A1	10.45°
A2	1.44°
B1	9.45°
B2	4.12°

scheme (in the ξ -direction) instead of the time marching scheme. Thus its application is restricted by the conditions involved in the PNS. The CPU time was about 2.25 hours on the IBM 3081 for an 83×41 mesh. The CPlot code is used for plotting the various variables obtained by running STARS3D through either a SURFACEII or a FORTRAN basic graphic routine. This also calculates approximate solutions by means of the HSDT. In addition, PLOT3D developed by NASA is utilized for entropy contours and some other plots.

4. GRID GENERATION AND GRID TYPES

Among various requirements of grid, smoothness and good grid control are basically important. The elliptic grid generation is one of the most widely used schemes. This can produce very smooth grids and they can be controlled by the inhomogeneous source terms (called control functions) in the Poisson's equations which are used for grid construction. It is not trivial to decide those control functions, while it is an important step. In this investigation, the control functions are determined by the following two factors; the grid control near the wall and the adaptive grid. The grid structure near the sharp tip plays a very crucial role in the numerical integration. An O-Type grid has an undesirable grid feature for this problem, since the grid lines of constant η around the tip are skewed too much. We introduce a *Fan-Type* grid where several rays come out of the same tip point. A typical *Fan-Type* grid for the leading-edge area is shown in Fig. 3. This will not cause any problem in numerically integrating the governing partial differential equations, since we are using a finite-volume method (FVM) and there is no flux in the body due to the zero cell area at the tip. Considering that the numerical algorithm is the 2nd order accurate in the crosswise direction and thus four cells are involved to calculate a flux, it is desirable to get at least four triangular grid cells. However, increasing the ray number for that purpose will make the cell areas smaller and thus the smooth variation of cell areas is deteriorated. This can be alleviated by introducing a point source at the tip which is determined by trial and error.

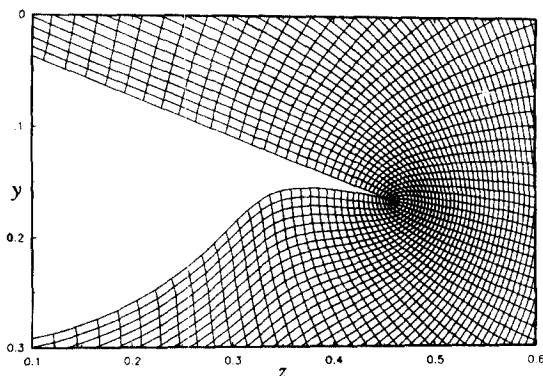


Fig. 3 *Fan-type* grid

5. DISCUSSIONS

Figure 4 shows the normalized-pressure distribution along the

waverider surface p_w/p_∞ versus the normalized horizontal axis $z/x \tan \delta$. It is for Model-A10 waverider using O-Type grid with 83×41 mesh (denoted by A10) and its leading-edge tip angle Δ_l is 10.45° . For the computer computations, the z coordinate is measured at the location $x=0.05$, where all the other numerical calculations are also carried out throughout this study. Since the flow and body are conical, the picture is similar in every vertical plane. The higher-pressure line in the figure is for the waverider lower-compression surface, and the lower-pressure line is for the upper-freestream surface. Strictly speaking, the pressure is for a half grid spacing above the wall. For the wall pressure the zero gradient assumption in the normal direction from the wall is used. As z increases, the pressure of the lower waverider surface also increases. This is mainly due to the larger deflection angle effect from the minor axis to the major axis of the elliptic cone which is the waverider generator. For the same pressure line we can see the region where the pressure decreases as z increases. Near the leading-edge, the pressure of the under-compression area increases as z increases, and it has the peak value right before reaching the edge. On the other hand, according to the analytical calculation (Rasmussen, 1991), the pressure for the same region decreases as z approaches the tip. To check whether the numerical pressure has the trend of the analytical calculation or not, we calculated the flow by using a more clustered grid near the tip and also *Fan-Type* grids. But the pressure increasing trend remained almost the same. In other words, the behavior of the numerical solutions near the tip does not match that of the approximate solution, while the flow for the rest of the tip region remains nearly unchanged and shows good agreement with HSDT. Figures 4,5 shows a comparison of the bow shocks for Model-A10 waverider as calculated by means of the hsdT and as captured by the numerical integration. The computational shock position was defined by the locations where the largest pressure gradient for each constant η line occurs. The shock captured by the computation is found to stand off from the leading-edge

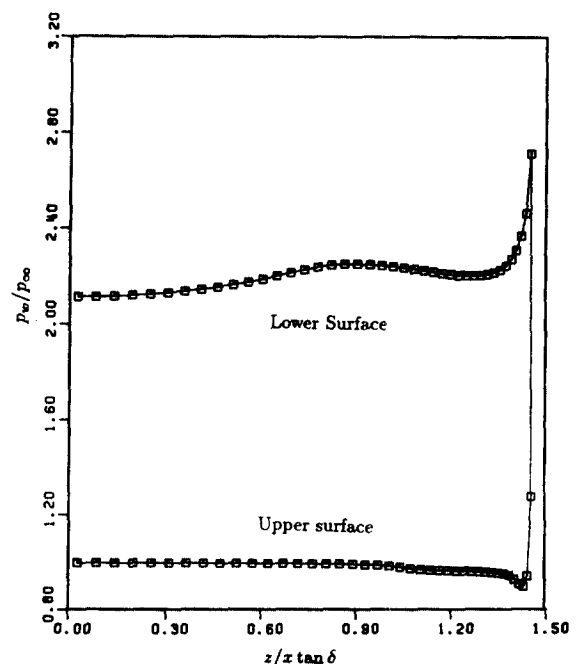


Fig. 4 Wall pressure distribution (Model-A10)

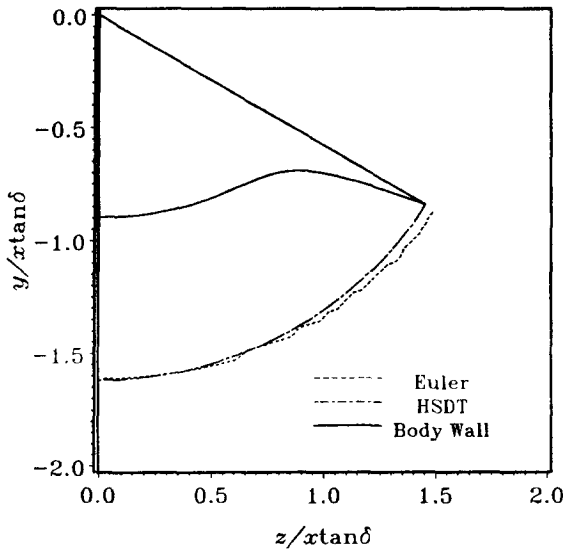


Fig. 5 Shock location comparison (Model-A1O)

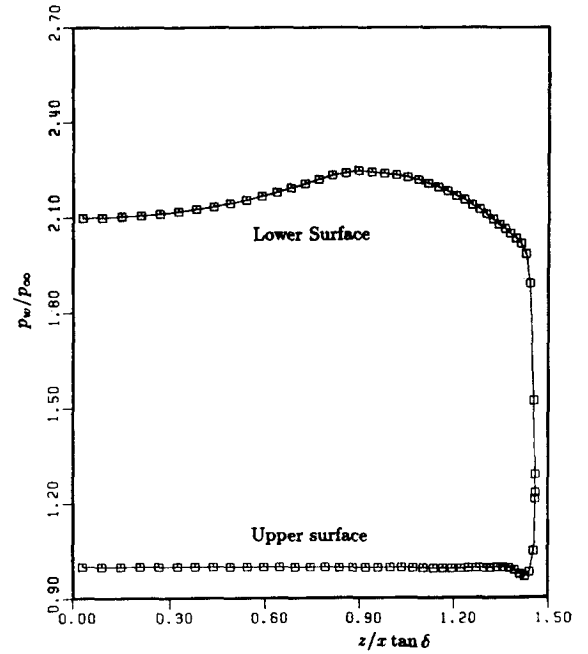


Fig. 7 Wall pressure distribution (Model-A2F)

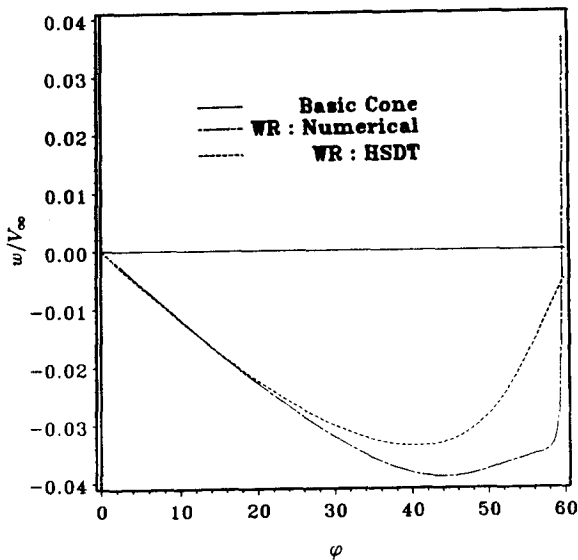


Fig. 6 Azimuthal velocity component (Model-A1O)

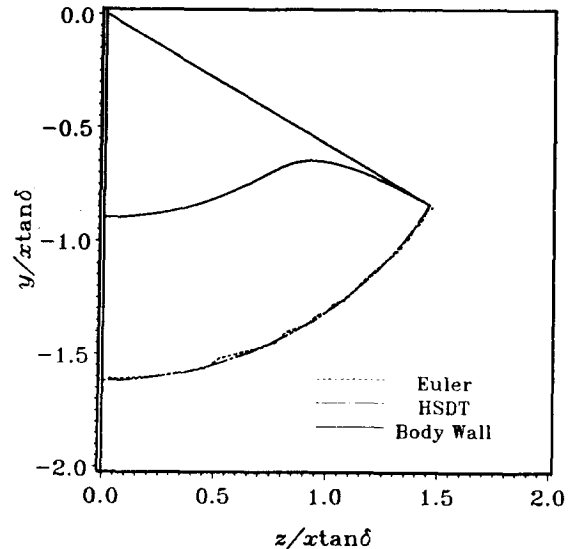


Fig. 8 Shock location comparison (Model-A2F)

instead of being attached, which should be for the ideal on-design condition. The attached shock can be expected only if the waverider geometry is based on the exact solution to the corresponding elliptic-cone flow and the solution to the flow past such a waverider is also exact. Thus, if either or both of the two conditions are not met, we cannot expect an attached shock in general. The waverider configuration used in this investigation is generated by means of an HSDT approximation. Through the gap between the leading-edge and the shock, the flow appears to be spilling from the lower region to the upper region owing to the large pressure gradient in the circumferential direction. As a result, the lift become smaller due to the reduced pressure in the shock layer. The azimuthal (ϕ) velocity components w for Model-A1O waverider are shown in Fig. 6. The analytic value of w

for the elliptic-cone flow has the term $\sin 2\phi$ (Rasmussen, 1991) which is different from the rest of the dependent variables. The maximum value of the ϕ -velocity component lies at $\phi \cong 45^\circ$ where the other perturbation variables vanish. Near the tip region, a relatively large discrepancy between the HSDT and the numerical calculation is detected. The much smaller numerical value of w from the computation is caused by the large pressure gradient in that region. The waverider wall pressure distribution for Model A2 waverider using Fan-Type grid with 83×41 mesh (denoted by A2F) is shown in Figs. 7,8,9. Its leading-edge tip angle Δ_2 is 1.44° . This shows no pressure peak at the tip, unlike the case in Fig. 4 and represents the same phenomena as what we anticipated for the waverider flow at the ideal on-design condition. The shocks for Model-A2F waverider by the HSDT and the

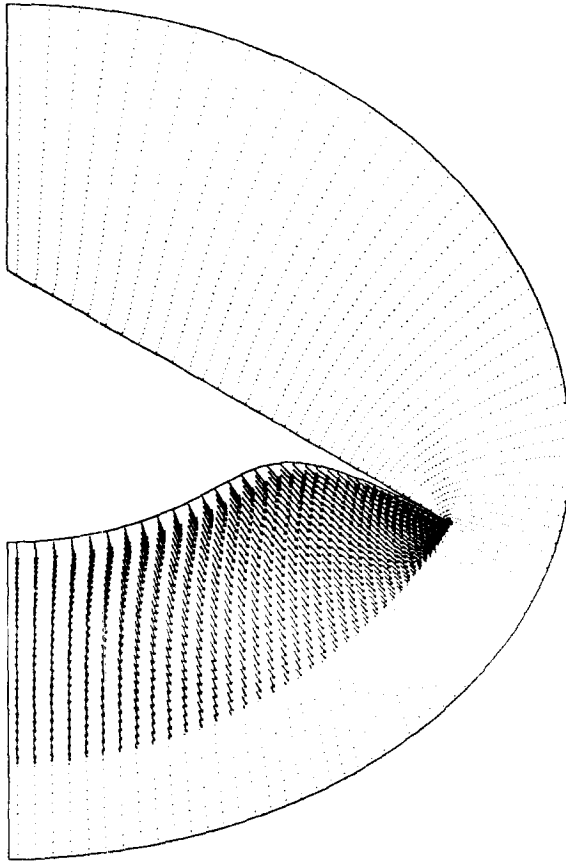


Fig. 9 Cross-plane velocity distribution (Model-A2F)

numerical solution are depicted in Fig. 8. This shows an amazingly good agreement between them, unlike the case of the Model-A1 waverider in Fig. 5. From the comparison of the shock locations in Figs. 5 and 8 we can assert that the reason for the large discrepancy for the shock locations in the Fig. 5 near the tip region is from the huge discrepancy of the waverider tip angles (compare Δ_1 with Δ_2). The nearly attached shock makes the lower high pressure flow region to be confined in the shock layer, which can be reconfirmed in the following figure. The cross-plane velocity distribution for Model-A2F is shown in Fig. 9. We can see that the flow disturbance near the tip region is very minor. This means that the shock is nearly attached at the tip, which is the desired result for the ideal on-design condition. Figure 10 shows the normalized pressure near the lower symmetry plane with different mesh sizes versus the normalized vertical length $y/x \tan \delta$. The numerical calculation for Model-B1 waverider was obtained by using O -Type grid (83×41 mesh). The shock locations are almost identical. The wider shock structure denoted by the dotted line is due to the worse resolution by the coarse grid. Figure 11 shows the comparison of the wall pressure coefficients C_p for B10 waverider by several researchers including the present study as functions of the azimuthal angle ϕ . The experimental data by Jischke et al. (Jischke, Rasmussen, Daniel, 1983) are plotted in the figure. There is a noticeable discrepancy between the experimental and present numerical data. The similar discrepancy between the experimental and the Euler numerical data by Liao et al. (Liao, Isaac, Miles, 1990) can be observed. In fact, a complete agreement cannot be reached, since the experimental data

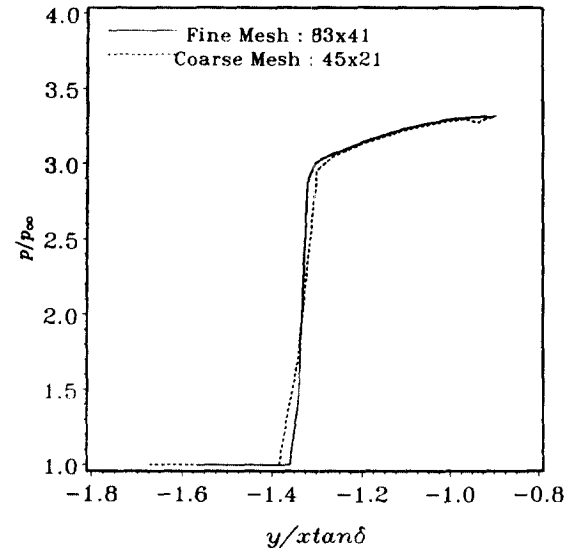


Fig. 10 Mesh size effect for shock (Model-B10)

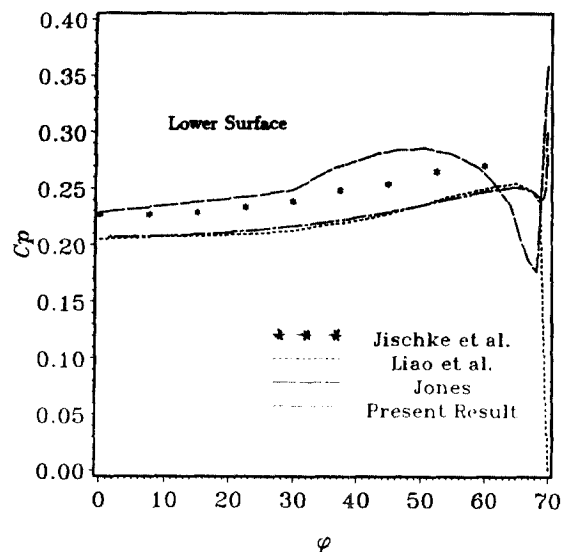


Fig. 11 Wall pressure coefficients. (Model-B10)

are related to the real viscous flow. However, except for this basic difference of the viscous and inviscid flows, it is difficult at the present time to explain very well the reason for the discrepancy in C_p . In spite of this disagreement in magnitude between the experimental and computational data, the comparison shows very similar trends for the range of the given experimental data points. Furthermore, a very good agreement between the numerical results by Liao et al. and the present investigation can be found except for the very small region near the leading-edge. The two results are obtained by completely different numerical integration methods. The above considerations on the trend and agreement lend confidence to the reliability of the present numerical results. In the figure the pressure coefficient by Jones (Jones, 1986) is also plotted. These data show better agreement with the experimental data for the lower values of ϕ , but for the higher values they do not. The trend shows somewhat irregu-

lar variation at $\phi \geq 30^\circ$.

6. CONCLUSIONS

Unlike some other researches appeared recently, we adopted steady equations for the computation of hypersonic flows past a class of elliptic-cone derived waveriders. This would require much hard labor than the use of unsteady equations but have great advantage such that we can save the computer storage and CPU time and thus the computation of waverider flows for a wide range of conditions would be also possible without paying much cost. By the comparison with the pressure coefficients of previous several researches we could be convinced of the numerical calculation results. In the process of numerical integration, various types of grid were tried for a converged solution and a *Fan*-Type grid which was developed in this research was quite successful. The bow shock at the nominal on-design conditions stands off from the leading-edge tip of the waverider (Model-*A1O*). It was found that this occurs because the tip was too thick according to the approximating formula that was used to describe the compression surface. This was confirmed by introducing a new formula (Model-*A2F*). This means the tip angle discrepancy near the tip is huge ($\Delta_1 \cong 7, 3\Delta_2$), although the overall error is the order of $\varepsilon^2(0.01)$ which is reasonably small. This large error near the tip which was unexpected at an earlier stage of this research is due to the singular nature of the sharp leading-edge. When this was corrected, we could get the desired result, that is, the bow shock became closer to attached as it should be.

ACKNOWLEDGMENTS

This work was supported by NASA Langley Grant No. NAG-1-886. The author really appreciate the support.

REFERENCES

- Jischke, M.C., Rasmussen, M.L. and Daniel, D.C., 1983, "Experimental Surface Pressures on Cone-Derived Waveriders for $M_\infty=3-5$," J. of Spacecraft and Rockets, Vol.20, No.6, Nov. Dec., pp.539~545.
- Jones, K.D. and Dougherty, F. C., 1990, "Computational Simulation of Flows about Hypersonic Geometries with Sharp Leading Edges," AIAA Paper 90-3065-CP, 8th Applied Aerodynamics Conference, Aug. 20~22, Portland, Oregon.
- Jones, K.M., 1986, "Application of a Supersonic Full Potential Method for Analysis of Waverider Configurations," NASA Technical Paper 2608.
- Lawrence, S.L., Tannehill, J. C. and Chaussee, D.S., 1986, "An Upwind Algorithm for the Parabolized Navier-Stokes Equations," AIAA Paper 86-1117.
- Liao, J.R., Isaac, K.M. and Miles, J.B., 1990, "Navier-Stokes Simulation of Waverider Flowfields," AIAA Paper 90-3066-CP, 8th Applied Aerodynamics Conference, Aug. 20~22, Portland, Oregon.
- Long, L.N., 1990, "Off-Design Performance of Hypersonic Waveriders," J. of Aircraft, Vol.27, No.7.
- Rasmussen, M.L., 1991, Textbook in preparation for John Wiley & Sons, "A Course in Hypersonic Flow."
- Rasmussen, M.L., 1986, "Experiments on a Slender Waverider Configuration with and without Inlet," Air Force Armament Laboratory Report AFATL-TR-86-07, Eglin AFB, FL.
- Rasmussen, M.L., 1980, "Waverider Configurations Derived from Inclined Circular and Elliptic Cones," J. of Spacecraft and Rockets, Vol.17, No.6, Nov. Dec., pp.537~545.
- Yoon, B-H., 1990, "Computational Analysis of Hypersonic Flows past Elliptic-Cone Waveriders," Ph. D.Dissertation, The Univ. of Oklahoma.